IEEE Access
Multidisciplinary | Rapid Review | Open Access Journal

Received March 29, 2019, accepted May 2, 2019, date of publication May 7, 2019, date of current version May 29, 2019.

Digital Object Identifier 10.1109/ACCESS.2019.2915308

Comprehensive Coordinated Control Strategy of PMSG-Based Wind Turbine for Providing Frequency Regulation Services

XUEYANG ZENG[1], TIANQI LIU[1], (Senior Member, IEEE), SHUNLIANG WANG[1], (Member, IEEE), YUQING DONG[1], AND ZHE CHEN[2], (Fellow, IEEE)

[1]College of Electrical Engineering and Information Technology, Sichuan University, Chengdu 610065, China
[2]Department of Energy Technology, Aalborg University, 9220 Aalborg, Denmark

Corresponding author: Tianqi Liu (tqliu@scu.edu.cn)

This work was supported by the National Key Research and Development Plan of China (No. 2018YFB0904600).

ABSTRACT A high proportion of wind energy in modern power system requires wind turbines (WTs) to provide frequency regulation services. In this context, this paper proposes a comprehensive coordinated control strategy of permanent magnet synchronous generator (PMSG)-based WT for providing an inertial response and primary control. First, a DC-link inertia control is proposed for providing virtual inertia by using the electrostatic energy stored in the DC capacitor, and the key parameters that affect the virtual inertia provided by this control are discussed in detail. Moreover, in order to provide more virtual inertia, a virtual capacitor control (VCC) strategy is proposed. With the VCC strategy, the rotor-side converter (RSC) can provide a virtual capacitance much larger than the actual DC capacitance and supply fast and transient extra power support by using the WT's rotor kinetic energy, in a similar way with the synchronous generator (SG) inertial response. Power-frequency droop control is adapted to allow WT to provide primary control service by using the WT's rotor kinetic energy. Furthermore, the virtual inertia constant of the proposed strategy is analytically derived. Finally, the simulation results in PSCAD/EMTDC are presented to verify the effectiveness of the proposed control strategy.

INDEX TERMS DC-link inertia control, frequency regulation, PMSG, power-frequency droop control, virtual capacitor control, virtual inertia support.

NOMENCLATURE

i	AC line current
P_{RS}	Active power output by PMSG
Q_{RS}	Reactive power output by PMSG
V_{ac}	AC grid voltage
V_{dc}	DC voltage of wind turbine (WT)
P_{wind}	Mechanical power extracted from the wind
P_{WT}	Power output by PMSG-based WT to AC system
ρ	Air density
R	Rotor blade radius
v_w	Wind speed
β	Pitch angle
C_p	Wind power utilization coefficient
$C_p^{\max}$	Maximum wind power utilization coefficient
ω_r	Wind turbine rotor speed
$\omega_r^{\max}$	Upper limit of rotor speed
λ	Tip-speed ratio
P_{ref}	Power reference determined by maximum power point tracking (MPPT)
k_{opt}	MPPT curve coefficient.
ΔP_H	Electromagnetic power output by synchronous generator (SG) inertial response
ΔP_P	Electromagnetic power output by SG primary control
H_g	Inertia constant of SG
S_g	Rated apparent power of SG
R_P	Droop coefficient of SG.
f	Instantaneous frequency of AC grid
P_{M^*}	Mechanical power input by the prime mover
P_{E^*}	Electromagnetic power output by the SG

The associate editor coordinating the review of this manuscript and approving it for publication was Tariq Masood.

ΔP_1	Rotational kinetic energy absorbed or released from the inertial response of SG
ΔP_2	Dynamic electrostatic power stored or released by DC capacitor.
C_{dc}	DC capacitance of WT
S_{WT}	Rated apparent power of WT
P_{in*}	Power flowing from RSC to DC capacitor in pu
P_{out*}	Power flowing from DC capacitor to GSC in pu
P_{in}	Power flowing from RSC to DC capacitor in MW
P_{out}	Power flowing from DC capacitor to GSC in MW
H_{dc}	Virtual inertia constant provided by DC capacitor
$\Delta f_{\max}$	Maximum allowed AC frequency deviation
$\Delta V_{\max}$	Maximum allowed DC voltage deviation
P_{ref_VCC}	Active power reference considering virtual capacitor control (VCC)
C_{vir}	Virtual capacitance
$\Delta P'_{vir}$	Additional power output provided by VCC
ΔP_R	Additional power provided by droop control
P^*_{ref}	Active power reference considering the power-frequency droop control and VCC
H_S	Inertia constant of WT, including the rotor constant and generator constant.
H_r	Virtual inertia constant provided by WT's rotor kinetic energy
P_{WT0}	WT output active power before the disturbance
H_{WT}	Total virtual inertia constant provided by the WT's rotor kinetic energy and the DC capacitor electrostatic energy

A. Superscripts

*	Reference value
ref	Reference value

B. Subscripts

d, q	d-axis and q-axis value
0	Nominal value

I. INTRODUCTION

In recent years, wind energy has developed rapidly due to climate change and energy crises. Wind energy is a clean energy source, but high proportion of which will bring new challenges to the frequency regulation of power system. This is because the output power of variable speed wind turbines (VSWTs) is usually controlled by the maximum power point tracking (MPPT) algorithm to maximize harvesting wind power, and the VSWTs are connected to the power grid through the power electronic converter, which decouple the rotation speed of VSWTs and the system frequency [1], [2]. So the inherent characteristics of the VSWT make it not participate in system frequency regulation. With the increasing proportion of wind energy in the power system, the system inertia will continue to decline, leading to greater challenges to frequency stability [3]–[5].

So far, in order to address this problem, various control strategies have been proposed to make use of the adjustment ability of the VSWT for frequency regulation, which can be categorized into three types. The first class is to utilize the pitch angle control to adjust the harvested energy [6]–[8]. However, it should be noted that the curtailed power is directly discarded and its response speed is relatively slow. In addition, frequent adjustment of the pitch angle may increase the mechanical stress and fatigue of the WT [9].

Another widely adopted strategy is to use the rotating kinetic energy stored in the WT's rotor to provide frequency regulation services, the advantages of which are as below: the response speed is faster than that of pitch angle control and a portion of the discarded power can be stored in the WT's rotor as rotational kinetic energy [9]. This frequency regulation scheme involves three types of implementation methods, including power-frequency droop control [2], [3], [10]–[13] based on system frequency deviation, derivation control [10]–[14] by using the rate of change of frequency (ROCOF) as input signal, and de-loading control [15]–[18] by shifting the MPPT curve to the right sub-optimal curve. The power-frequency droop control simulates the primary control of the synchronous generator (SG), which aims to provide continuous active power support that responds to the frequency deviation and to improve the frequency nadir. Derivation control emulates the inertial response of SG, the purpose of which is to provide virtual inertia support during the initial stage of the disturbance. But it may cause system instability because the signal it inputs is the derivative of system frequency, which may lead to measurement noise [3]. In addition, Derivation control may affect the system dynamic process, and the WT does not provide frequency support when the system frequency reaches the maximum or minimum, so derivation control cannot be utilized alone for system frequency regulation [2]. The VSWTs can obtain power reserve under the de-loading control, but the captured wind energy will inevitably be lost because the harvested wind energy is not maximized [3], [15].

The last scheme is to utilize the electrostatic energy stored in the DC capacitor of VSWT to provide virtual inertia support [3], [9], [19], [20]. Compared with the above two approaches, the DC-link voltage control is the most preferred choice because it never affects MPPT control, while the available DC capacitor energy is relatively small. Literatures [3], [19], and [20] introduce DC voltage-frequency droop control in converter control, which can adjust the DC voltage reference following the AC frequency fluctuations to release or absorb the electrostatic energy in the DC capacitor. Literatures [9] and [21] use the energy stored in the DC capacitor to smooth the fluctuating output power, essentially by changing the DC voltage reference. Although the studies

above indicate that the electrostatic energy stored in a DC capacitor can provide virtual inertia support, but it has not been discussed how to set the droop coefficient and the key factors affecting the virtual inertia support provided by DC capacitor.

Focusing on providing virtual inertia support and primary control from permanent magnet synchronous generator (PMSG)-based WT, this paper proposes a comprehensive coordinated control strategy that makes full use of the WT's own potential to participate in frequency regulation. Firstly, a DC-link inertia control is proposed by establishing the coupling relationship between DC voltage and AC frequency. Then it is discussed in detail how to choose the key factors, which affect virtual inertia and droop coefficient. The results show that even by increasing the DC capacitance and the allowed DC voltage deviation, the virtual inertia provided by this control method is still small. To overcome this problem, a virtual capacitor control (VCC) strategy is proposed, which can provide a virtual capacitor to support more virtual inertia support. In order to provide primary control service, a power-frequency droop control is adopted in WT system. With the proposed coordinated control strategy, the PMSG-based WT system is able to provide inertial response and participate in primary frequency regulation, by utilizing DC capacitor energy and WT's rotor kinetic energy simultaneously, in a similar way with the SG. Furthermore, the virtual inertia constant of the proposed strategy is analytically derived, and the influence of each control method on virtual inertia support is discussed.

The paper is organized as follows: Section II introduces the PMSG-based WT system model in this study and principle of power system regulation. The DC-link inertia control is proposed in Section III. Section IV presents the virtual capacitor control and power-frequency control. Section V derives the virtual inertia time constant of this coordinated control strategy. Simulation results are given to validate the proposed coordinated control strategy in section VI. Conclusions are summarized in section VII.

II. PMSG-BASED WT MODLE AND POWER SYSTEM FREQUENCY REGULATION

A. PMSG-BASED WT MODLE

The schematic diagram of PMSG-based wind turbine (WT) system is shown in Fig. 1. The PMSG-based WT is connected to power system through a full-scale back-to-back converter, where the rotor-side converter (RSC) controls the generated active power and the grid-side convertor (GSC) is used to control DC-link voltage [22], [23]. In normal operation, the active power generated by the WT is achieved by maximum power point tracking (MPPT) algorithm and pitch angle control [3].

The mathematical expression of the mechanical power P_{wind} extracted from the wind is described as follows [24],

$$P_{wind} = \frac{1}{2}\pi\rho R^2 v_w^3 C_P(\lambda, \beta) \tag{1}$$

$$\lambda = \frac{\omega_r R}{v_w} \tag{2}$$

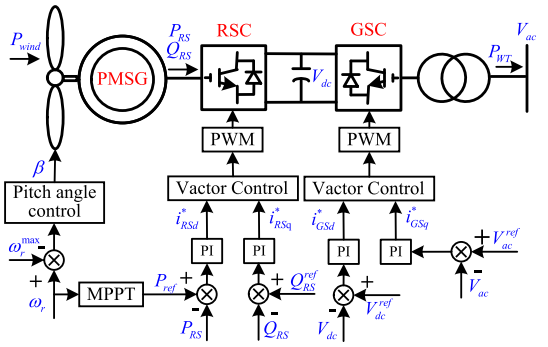

FIGURE 1. Schematic diagram of PMSG-based WT system.

where ρ is air density, R is the rotor blade radius,v_w is the wind speed, λ is the tip-speed ratio, β is the pitch angle, Cp is the wind power utilization coefficient, ω_r is the wind turbine rotor speed, Normally, when ω_r is below the upper limit of rotor speed $\omega_r^{\max}$, the pitch angle is zero, then C_p is a function only related to λ, and it will reach the maximum value $C_p^{\max}$ [17], [25].

Bring (2) into (1), yields,

$$P_{ref} = \frac{\pi\rho R^5 C_p^{\max}}{2\lambda^3}\omega_r^3 = k_{opt}\omega_r^3 \tag{3}$$

where P_{ref} is active power reference value determined by MPPT algorithm, k_{opt} is the MPPT curve coefficient.

B. POWER SYSTEM FREQUENCY REGULATION

The power imbalance between load and power generation will cause frequency fluctuations in an AC grid. When this phenomenon occurs, the conventional SG would thus adjust its power transmitted to the AC grid to offer frequency support. The kinetic energy stored in the rotor of the SG will quickly change following the variation of frequency, where the released or absorbed kinetic energy will result in the increase or decrease of the output electromagnetic power. The part of the electromagnetic power generated by the inertial response of the SG is proportional to the rate of change of frequency (ROCOF) [26]. It is noted that the inertial response plays a major role in hindering the ROCOF during the first few seconds after a disturbance occurs. After a few seconds, the primary control starts working and the frequency ends up in reaching a new equilibrium point. A few minutes later, the secondary control will be activated to adjust the frequency to the normal value [26], [27].

The electromagnetic power output ΔP_H by SG inertial response and ΔP_P by primary control can be calculated as in (4) and (5), respectively.

$$\Delta P_H = -\frac{2H_g S_g}{f_0^2} f\frac{df}{dt} \approx -\frac{2H_g S_g}{f_0}\frac{df}{dt} \tag{4}$$

$$\Delta P_P = -\frac{1}{R_P}(f - f_0) = -\frac{1}{R_P}\Delta f \tag{5}$$

where, H_g is the inertia constant of SG, S_g is the rated apparent power of SG, f_0 is the nominal frequency of the grid,

f is the measured instantaneous frequency of AC grid, Δf is the frequency difference, R_P is the droop coefficient of SG.

The function of inertia response is to hinder the ROCOF, prevent the system frequency from falling rapidly, and gain time for primary control. The primary control aims at supplying continuous active power support that responds to the frequency deviation, so as to prevent the continuous drop of the system frequency and allow frequency to achieve a new balance.

III. DC-LINK INERTIAL CONTROL

The WT output power is usually controlled by the MPPT algorithm and insensitive to the grid frequency changes because of the full-scale back-to-back converter. In addition, the DC voltage controlled by the GSC is a constant and decoupled from AC frequency, so the kinetic energy stored in the WT's rotor and the electrostatic energy stored in the DC capacitor will not participate in the frequency regulation. To address this problem, this section proposes a DC-link inertia control by coupling AC frequency to the DC-link voltage of converter in WT system, allowing the electrostatic power stored in the DC capacitor to provide inertial support for the power system.

For the AC system, the typical rotor motion equation of the SG can reflect the dynamic response of frequency as described in

$$\frac{2H_g}{f_0}\cdot\frac{df}{dt}=P_{M^*}-P_{E^*}=\Delta P_1(\text{pu}) \tag{6}$$

where P_{M^*} is the mechanical power input by the prime mover, P_{E^*} is the electromagnetic power output by the SG, ΔP_1 is the rotational kinetic energy absorbed or released from the inertial response of SG during the speed change.

For the back-to-back converter, the DC voltage variations can reflect the power imbalance, similar to frequency in an AC system. Ignoring the power loss, the dynamic equation of DC capacitor, similar to (6), is shown in (7).

$$\frac{C_{dc}V_{dc}}{S_{WT}}\cdot\frac{dV_{dc}}{dt}=P_{in^*}-P_{out^*}=\Delta P_2(\text{pu}) \tag{7}$$

where C_{dc} is the DC capacitance of WT system, V_{dc} is the measured DC voltage, S_{WT} is the rated apparent power of the WT, P_{in^*} is the power flowing from RSC to DC capacitor in pu, P_{out^*} is the power flowing from DC capacitor to GSC in pu, ΔP_2 is the dynamic electrostatic power stored or released by DC capacitor.

A relationship between DC voltage and AC frequency is established by making (6) and (7) equal, thus the electrostatic power stored in the DC capacitor can provide inertial support for the power system [28]. And then integrating both sides with respect to time yields

$$\int_{f_0}^{f}\frac{2H_{dc}}{f_0}df=\int_{V_{dc0}}^{V_{dc}}\frac{C_{dc}V_{dc}}{S_{WT}}dV_{dc} \tag{8}$$

$$\frac{2H_{dc}(f-f_0)}{f_0}=\frac{C_{dc}(V_{dc}^2-V_{dc0}^2)}{2S_{WT}} \tag{9}$$

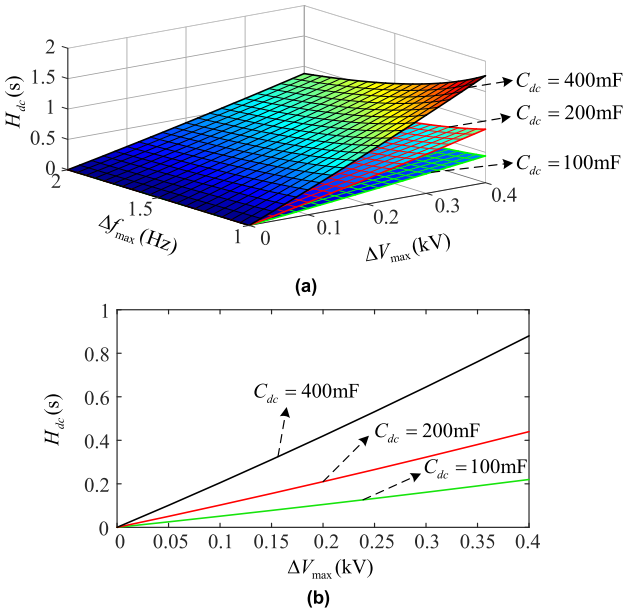

FIGURE 2. Relationship among virtual inertia constant H_{dc}, maximum allowed frequency and voltage deviation (Δf_{max}, ΔV_{max}), DC capacitance C_{dc}. (Using the WT's parameters in Appendix Table 3).

where H_{dc} is the virtual inertia constant provided by DC capacitor, V_{dc0} is the nominal DC voltage.

The virtual inertia constant H_{dc} and the DC voltage reference V_{dc}^* in GSC constant DC voltage control can be obtained from (9). The relationship among H_{dc}, maximum allowed frequency and voltage deviation ($\Delta f_{\max}$, $\Delta V_{\max}$), DC capacitance C_{dc} is depicted in Fig. 2.

$$H_{dc}=\frac{C_{dc}f_0V_{dc0}^2}{4S_{WT}\Delta f_{\max}}\left[\left(\frac{\Delta V_{\max}}{V_{dc0}}+1\right)^2-1\right] \tag{10}$$

$$V_{dc}^*=\sqrt{\frac{4H_{dc}S_{WT}(f-f_0)}{f_0C_{dc}}+V_{dc0}^2} \tag{11}$$

where $\Delta V_{\max}$ is the maximum allowed DC voltage deviation, and $\Delta f_{\max}$ is the maximum allowed frequency deviation.

Since the frequency varies within a small range (restricted within $\pm$0.05pu), (11) may be linearized around its equilibrium point by Taylor Expansion. Therefore, V_{dc}^* can be expressed as (12) after ignoring the higher order items. The relationship among voltage variation ΔV_{dc}, virtual inertia constant H_{dc}, frequency variation Δf,and DC capacitance C_{dc} is shown in Fig. 3. The block diagram of the DC inertia control is shown in Fig. 4.

$$V_{dc}^*=V_{dc0}+\frac{2H_{dc}S_{WT}}{V_{dc0}f_0C_{dc}}(f-f_0)=V_{dc0}+K_{dc}(f-f_0) \tag{12}$$

Substituting H_{dc} in (10) into (12), yields,

$$K_{dc}=\frac{2H_{dc}S_{WT}}{V_{dc0}f_0C_{dc}}=\frac{V_{dc0}}{2\Delta f_{\max}}\left[\left(\frac{\Delta V_{\max}}{V_{dc0}}+1\right)^2-1\right] \tag{13}$$

Equation (12) indicates that after linearization of (11), DC-link inertia control is essentially a droop control, and the droop coefficient can be determined by (13).

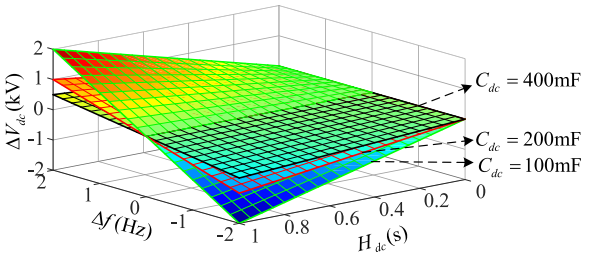

FIGURE 3. Relationship among voltage variation ΔV_{dc}, virtual inertia constant H_{dc}, frequency variation Δf, and DC capacitance C_{dc}. (Using the WT's parameters in Appendix Table 3).

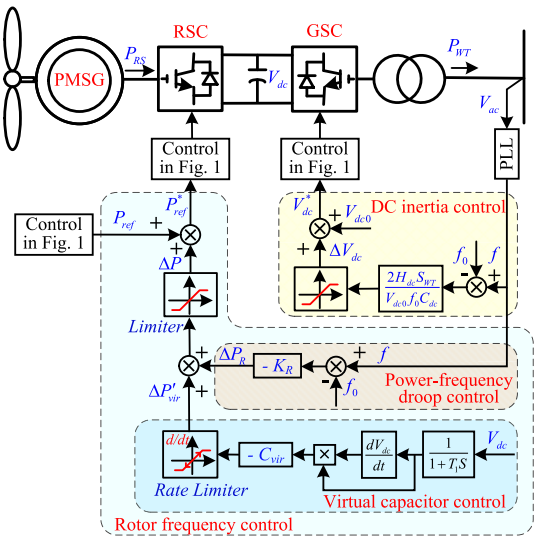

FIGURE 4. Control diagram of the proposed coordinated control strategy.

It can be clearly seen from (10) and Fig. 2(a) that increasing C_{dc}, $\Delta V_{\max}$, or reducing $\Delta f_{\max}$ seems to enhance H_{dc}. However, it should be noted that $\Delta f_{\max}$ is determined by the power equipment such as generators, transmission networks, loads and so on, and is not controlled by the WT system. So only by increasing C_{dc} and $\Delta V_{\max}$ can improve H_{dc}. This paper considers that WT is connected to a relatively weak power grid, so $\Delta f_{\max}$ is selected as 2Hz. Moreover, as shown in (13), the promotion of $\Delta V_{\max}$ is equivalent to the enhancement of K_{dc}. With the same frequency deviation, more DC capacitor energy can be released or absorbed.

In addition, from Fig. 3, for a specific Δf and a fixed C_{dc}, the increase of H_{dc} will result in a larger ΔV. This is because C_{dc} is a fixed value, the improvement of H_{dc} can only be achieved by increasing $\Delta V_{\max}$. It can be concluded from (10) and (13) that for a specific Δf, increasing C_{dc} can provide a suitable virtual inertia constant H_{dc} without improving ΔV, because K_{dc} is a function unrelated to C_{dc}, but it will increase the cost and converter volume. What's more, the increase of $\Delta V_{\max}$ may lead to insulation and modulation issues. From Fig. 2(b), even if the C_{dc} is increased to 400mF (C_{dc} is usually around 100mF) and $\Delta V_{\max} = 0.4$kV (0.2pu), the virtual inertia constant produced by the DC-link capacitor is still

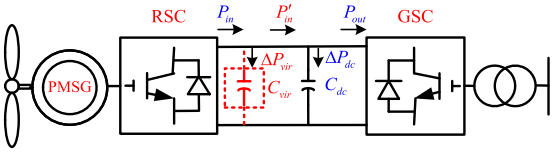

FIGURE 5. Analysis diagram of back-to-back converter virtual capacitor.

less than 1s, which is smaller than that provided by the SG (H_g normally ranges from 2s to 10s [29], [30]). Therefore, it is obviously uneconomical and unnecessary to provide the required virtual inertia constant by increasing the DC capacitance.

IV. WT ROTOR FREQUENCY CONTROL

As analyzed in the previous section, the inertia provided by the normal DC capacitor is very limited, and it may cause excessive DC voltage deviation. Therefore, to provide the required virtual inertia constant and keep the DC voltage within a safe range, larger capacitance is needed for the WT system, but it will increase the cost and converter volume.

The WT's rotor kinetic energy is much greater than the electrostatic energy stored in DC capacitor. However, the output power of WT is controlled by MPPT algorithm, and there is no direct relationship between the rotor speed ω_r of WT and AC frequency f because of the full-scale back-to-back converter, which causes the rotational kinetic energy to be hidden and contributes little to frequency regulation services for power grid. To solve this problem, a novel VCC strategy is proposed in this section to provide a reasonable virtual capacitance and improve the power system inertia. In addition, in order to provide primary control service, a power-frequency droop control is adopted in WT.

A. VIRTUAL CAPACITOR CONTROL

Fig.5 shows the diagram of system power balance with DC capacitor. Multiplying both sides of equation (7) by the rated apparent power S_{WT}, the relationship between the DC voltage and the DC power can be obtained as (14) during a disturbance.

$$C_{dc}V_{dc}\frac{dV_{dc}}{dt} = P_{in} - P_{out} \tag{14}$$

where P_{in} is the power flowing from RSC to DC capacitor in MW, P_{out} is the power flowing from DC capacitor to GSC in MW.

It can be seen from (14) that when the WT operates in a steady state, the DC voltage is maintained at a constant value. During a disturbance, the larger DC capacitance, the smaller voltage change rate dV_{dc}/dt and the greater virtual inertia support provided by the DC capacitor. However, limited by the actual DC capacitor capacity, this virtual inertia is small. Fortunately, a VCC strategy as shown in (15) is adopted in RSC to quickly adjust the input power at the moment of voltage fluctuation, so that the converter can quickly absorb or release the additional power ΔP_{vir}, as shown

in (16). The control diagram is shown in Fig. 4.

$$P_{ref\_VCC} = P_{ref} - \Delta P_{vir} = P_{ref} - C_{vir} V_{dc} \frac{dV_{dc}}{dt} \quad (15)$$

$$\Delta P_{vir} = C_{vir} V_{dc} \frac{dV_{dc}}{dt} \quad (16)$$

where, P_{ref_VCC} is the new active power reference value considering VCC strategy, C_{vir} is defined as the virtual capacitance because it is realized by the proposed VCC strategy in RSC.

Taking the ΔP_{vir} into account, the new input power flowing P'_{in} from RSC to DC capacitor is expressed as

$$P'_{in} = P_{in} - \Delta P_{vir} = P_{in} - C_{vir} V_{dc} \frac{dV_{dc}}{dt} \quad (17)$$

Substituting P'_{in} in (17) to P_{in} in (14) can obtain

$$(C_{dc} + C_{vir}) V_{dc} \frac{dV_{dc}}{dt} = P_{in} - P_{out} \quad (18)$$

Equation (18) indicates that adopting the proposed VCC strategy can be considered as adding a virtual capacitor C_{vir} in parallel with C_{dc}, as shown by the red dashed line in Fig. 5. And the capacity of virtual capacitor C_{vir} can be adjusted according to the required virtual inertia constant. Increasing the virtual capacitance C_{vir} can reduce the actual DC capacitance C_{dc} requirement, which can save cost and reduce the converter volume.

Derivation on both sides of (12) yields (19) below.

$$\frac{dV_{dc}}{dt} = \frac{2H_{dc}S_{WT}}{V_{dc0}f_0 C_{dc}} \cdot \frac{df}{dt} \quad (19)$$

The relationship between the additional power output $\Delta P'_{vir}$ of WT and AC frequency can be obtained from (18), and (19), as shown in (20).

$$\Delta P'_{vir} = -\Delta P_{vir} = -\frac{2C_{vir}V_{dc}H_{dc}S_{WT}}{V_{dc0}f_0 C_{dc}} \cdot \frac{df}{dt} \quad (20)$$

In practice, the DC voltage deviation is quite small (within ± 0.1pu in this paper), so the DC voltage V_{dc} is approximated to normal DC voltage V_{dc0} ($V_{dc} \approx V_{dc0}$). Equation (20) can be rewritten as (21).

$$\Delta P'_{vir} \approx -\frac{2C_{vir}H_{dc}S_{WT}}{f_0 C_{dc}} \cdot \frac{df}{dt} = -\frac{2H_{vir}S_{WT}}{f_0} \cdot \frac{df}{dt} \quad (21)$$

where H_{vir} is the virtual inertia constant provided by WT rotor due to VCC strategy, as shown in (22).

$$H_{vir} = \frac{C_{vir}H_{dc}}{C_{dc}} \quad (22)$$

Bring (10) into (22) yields

$$H_{vir} = \frac{C_{vir}f_0 V_{dc0}^2}{4S_{WT}\Delta f_{\max}} \left[\left(\frac{\Delta V_{\max}}{V_{dc0}} + 1 \right)^2 - 1 \right] \quad (23)$$

B. POWER-FREQUENCY DROOP CONRTOL

It can be derived from equation (21) that with VCC strategy, the extra power support provided by the WT is proportional to the ROCOF. So the WT can provide the virtual inertia support at the initial stage of the disturbance, but when the frequency deviation reaches the maximum, the ROCOF is zero, thus the inertia support provided by the WT is zero. What is worse is that during the frequency recovery process, the extra power support provided by the WT is opposite to that required by the power system.

To solve this problem, a power-frequency droop control shown in (24) is introduced into the WT system [2], [3], and [10]–[13]. The additional power ΔP_R provided by droop control is given in (25) and the control diagram is shown in Fig. 4.

$$P^*_{ref} = P_{ref\_VCC} + \Delta P_R = P_{ref} - C_{vir} V_{dc} \frac{dV_{dc}}{dt} - K_R (f - f_0) \quad (24)$$

$$\Delta P_R = -K_R (f - f_0) \quad (25)$$

where P^*_{ref} is the new active power reference value of WT considering the power-frequency droop control and VCC strategy, K_R is the droop coefficient.

V. VIRTUAL INERTIA CONSTANT OF PROPOSED COORDINATED CONTROL

The dynamic characteristics of the WT's rotor can be described by the rotor motion equation, as shown in (26).

$$2H_S\omega_r S_{WT} \frac{d\omega_r}{dt} = P_{wind} - P_{ref} \quad (26)$$

where, H_S is the inertia constant of WT, including the rotor constant and generator constant.

The core idea of the VCC strategy and the power-frequency droop control is to provide virtual inertia support by using WT's rotor kinetic energy. The active reference value P_{ref} of the WT will be replaced by a new one P^*_{ref} during a disturbance. Equation (26) can be rewritten as

$$2H_S\omega_r S_{WT} \frac{d\omega_r}{dt} = P_{wind} - P^*_{ref} \quad (27)$$

With the similar form in (6), (27) can be revised as follows,

$$\frac{2H_r S_{WT}}{f_0} \cdot \frac{df}{dt} = P_{WT0} - P^*_{ref} = P_{WT0} - (P_{ref} + \Delta P'_{vir} + \Delta P_R) \quad (28)$$

where H_r is the virtual inertia constant provide by WT's rotor kinetic energy (considering the VCC strategy and power-frequency droop control), P_{WT0} is the WT output active power before the disturbance.

Integrating both sides of (28) with respect to time yields,

$$\int_{f_0}^{f} \frac{2H_r S_{WT}}{f_0} \cdot \frac{df}{dt} = \int_{t_0}^{t} (P_{WT0} - P_{ref})dt - \int_{t_0}^{t} \Delta P'_{vir} dt - \int_{t_0}^{t} \Delta P_R dt \quad (29)$$

Bring (21) and (25) into (29), the virtual inertia constant H_r can be expressed as

$$H_r = \frac{f_0 \int_{t_0}^{t} (P_{WT0} - P_{ref})dt}{2S_{WT}\Delta f} + H_{vir} + \frac{f_0 \int_{t_0}^{t} K_R \Delta f dt}{2S_{WT}\Delta f} = H_1 + H_2 + H_3 \quad (30)$$

It can be seen from (30) that the virtual inertia constant H_r consists of three parts (H_1, H_2 and H_3). H_1 represents the influence of the MPPT curve on H_r. If the frequency drops ($\Delta f < 0$), VCC strategy and droop control will trigger a declining rotor speed to release kinetic energy. It can be seen from (3) that if the rotor speed decreases, the power reference P_{ref} will decrease, so the numerator of H_1 is positive and H_1 is negative [3], [25]. Obviously, H_2 is a constant, which reflects the effect of VCC strategy on H_r. H_3 indicates the effect of power-frequency droop control on H_r. Considering the small variation of frequency and rotor speed during the first few seconds after a disturbance occurs, H_1 and H_3 is approximately equal to zero. This means that the virtual inertia during this period is mainly provided by VCC. With the increase of Δf, the inertia H_3 provided by droop control is improving.

Combined with (10), (23) and (30), the total virtual inertia constant H_{WT} provided by the WT's rotor kinetic energy and the DC capacitor electrostatic energy is as follows,

$$H_{WT} = H_r + H_{dc} = \frac{f_0 \int_{t_0}^{t} (P_{WT0} - P_{ref})dt}{2S_{WT}\Delta f} + \frac{f_0 \int_{t_0}^{t} K_R \Delta f dt}{2S_{WT}\Delta f} + \frac{(C_{vir} + C_{dc}) f_0 V_{dc0}^2}{4S_{WT}\Delta f_{\max}} \left[\left(\frac{\Delta V_{\max}}{V_{dc0}} + 1 \right)^2 - 1 \right] \quad (31)$$

Obviously, the proposed coordinated control can provide greater virtual inertia support. The purpose of DC-link inertia control and VCC is to simulate the inertial response of SG, providing virtual inertia support during the initial stage of the disturbance, hindering the ROCOF and preventing the AC frequency from falling rapidly. The goal of power-frequency droop control is to simulate the primary control of SG, providing continuous active power support, preventing the continuous drop of AC frequency, improving the frequency nadir, and allowing frequency to achieve a new balance.

Fig. 4 shows the entire control diagram of the proposed coordinated control strategy. Taking the AC frequency reduction as an example, the DC-link inertial control of GSC firstly lowers its DC voltage reference value to release the electrostatic energy stored in the DC capacitor. At the same time, the reduction of DC voltage enables the VCC strategy of RSC to increase its active power output by releasing the WT's rotor kinetic energy. Meanwhile, with the increase of frequency deviation, the power-frequency droop control also increases WT's active power output by releasing the WTs' rotor kinetic energy. Through a series of actions of the above control, the WT can provide inertial response and primary control services, which can reduce the ROCOF and improve frequency nadir, thus enhance the overall system stability.

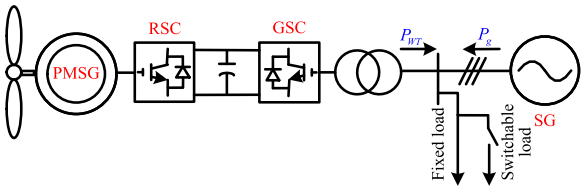

FIGURE 6. Single-line diagram of the simulation test system.

TABLE 1. Parameters and simulation results of different study case.

Case	Parameters				Simulation results
	C_{dc}	$\Delta V_{\max}$	$\Delta f_{\max}$	H_{dc}	$\lvert ROCOF \rvert_{\max}$*
1	100mF	0.1pu	2Hz	0.105s	0.757Hz/s
2	200mF	0.1pu	2Hz	0.21s	0.734Hz/s
3	400mF	0.1pu	2Hz	0.42s	0.702Hz/s
4	100mF	0.2pu	2Hz	0.22s	0.731Hz/s
5	100mF	0.3pu	2Hz	0.345s	0.709Hz/s
6	100mF	\	\	\	0.785Hz/s

* $\lvert ROCOF \rvert_{\max}$ is the maximum value of ROCOF absolute value.

What's more, the proposed coordinated control strategy does not require additional energy storage facilities.

VI. SIMULATION AND RESULTS

In order to verify the effectiveness of the proposed coordinated control, a simulation test system comprising of a PMSG-based WT, a SG, a fixed load and a switchable load is built in PSCAD/EMTDC, as shown in Fig. 6. The parameters of PMSG-based WT and SG are listed in Appendix Table 3 and Table 4, respectively. The fixed load is specified as 6MW + 0.6MVar, and the switchable load is chosen as 0.6MW + 0.06MVar, representing 10% fixed load. Wind speed is set as 10.1m/s and the switchable load is applied to power system at 10s to create the frequency dynamics.

A. DC-LINK INERTIA CONTROL WITH DIFFERENT PARAMETERS

In order to verify the effectiveness of DC-link inertia control with different parameters, a simulation example with six cases listed in Table 1 is designed. Cases 1, 2, and 3 show the influence of DC capacitance C_{dc} on virtual inertia constant H_{dc}. Cases 1, 4, and 5 illustrate the influence of maximum allowed DC voltage deviation $\Delta V_{\max}$ on H_{dc}. Case 6 represents without dc-link inertia control. The simulation results of the system responses with different parameters are shown in Fig. 7 and Table 1.

It can be observed from cases 1, 2, and 3 that a larger DC capacitance can provide more virtual inertia support without increasing DC voltage deviation, and can bring more improvements to ROCOF. Comparing Cases 1, 4, and 5, it can be known that by increasing the maximum allowed DC voltage deviation $\Delta V_{\max}$, DC capacitor would also provide more virtual inertia support and reduce ROCOF, but this will lead to DC voltage deviation increasing. The simulation results verify the influence analysis of C_{dc} and $\Delta V_{\max}$ on

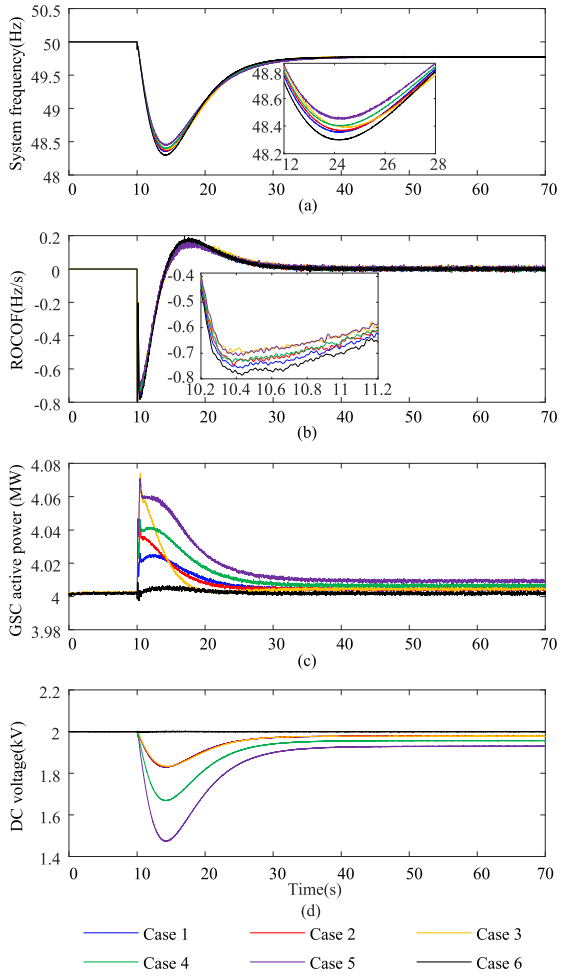

FIGURE 7. Simulation results for sudden load increase under DC-link inertia control. (a) System frequency. (b) ROCOF. (c) GSC active power. (d) DC voltage.

H_{dc} in section III. However, even if the C_{dc} is increased to 4 times the normal value or $\Delta V_{\max}$ is increased to 0.3pu, the virtual inertia provided by the DC capacitor is still very small, which brings very small improvements to the ROCOF and frequency nadir, as observed form Fig. 7(a) and Fig. 7 (b).

B. SUDDEN LOAD INCREASE UNDER DIFFERENT CONTROL METHODS

Five different control methods are listed in Table 2 and simulation results are compared in Fig. 8 and Table 2.

From the Fig. 8 and Table 2, it can be observed that DC capacitor and WT rotor cannot provide inertia support if without additional control, where DC voltage and rotor speed do not change during system transients. With DC-link inertia control, GSC can increase the injected active power by releasing the energy stored in the DC capacitor. However, as previously analyzed, the active power is limited because the normal DC capacitance is relatively small. It can only bring a little improvement in the ROCOF and frequency nadir, as shown in Fig. 8(a), Fig. 8(b) and Table 2. Compared

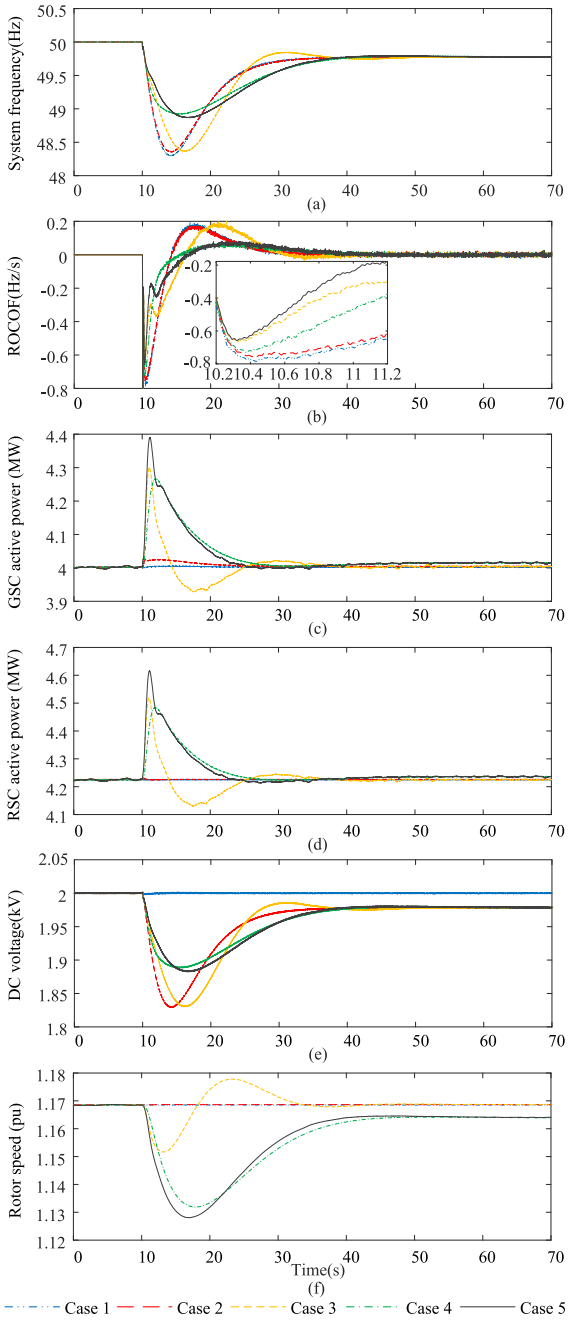

FIGURE 8. Simulation results for sudden load increase under different control methods. (a) System frequency. (b) ROCOF. (c) GSC active power. (d) RSC active power. (e) DC voltage. (f) Rotor speed.

with case 2 and case 3, using the proposed VCC strategy, the system frequency is dropping slower significantly, but the frequency nadir only improved a little. Moreover, it is noticed that in the process of system frequency recovery, the WT rotor absorbs the same amount of power to restore the rotor speed. This is because the extra power provided by the VCC strategy is proportional to ROCOF, as shown in (21). The WT absorbs some power for the speed recovery during the frequency recovery process. So the VCC is aimed to emulate the inertial response of SG, providing virtual

TABLE 2. Parameters* and simulation results of different study case.

Description	Simulation results	
	$\|ROCOF\|_{max}$	f_{nadir}*
Case 1: without any additional control	0.785Hz/s	48.30Hz
Case 2: with DC-link inertia control	0.757Hz/s	48.35Hz
Case 3: with DC-link control and VCC	0.664Hz/s	48.37Hz
Case 4: with DC-link and droop control	0.731Hz/s	48.97Hz
Case 5: with the proposed control	0.657Hz/s	48.91Hz

* Parameters:
DC-link inertia control: C_{dc}=100mF, Δf_{max}=2Hz, ΔV_{max}=0.1pu, H_{dc}= 0.105s.
VCC strategy: C_{vir}=3810mF, H_{vir}=4s.
Power-frequency droop control: K_R=0.5.
* f_{nadir} is the frequency nadir.

TABLE 3. Parameters of PMSG-based WT.

Item	Value
DC-link capacitance C_{dc}	100 mF
Rated DC-link voltage V_{dc0}	2 kV
Rated power S_{WT}	5 MW
Nominal frequency f_0	50 Hz
Rotor blade radius R	63 m
Inertia constant H_S	4 s
Damping coefficient	0.01 pu
Terminal voltage	690 V
Rated rotor speed	1.23 pu
Rated wind speed	11.3 m/s
Cut in wind speed	3 m/s
Cut out wind speed	25 m/s

TABLE 4. Parameters of the SG.

Item	Value
Rated MVA S_g	6 MVA
Terminal Voltage V_g	6.6 kV
Inertia time constant H_g	3.114 s
x_d , x'_d , x''_d	1.305, 0.296, 0.252
x_q , x''_q , x_l	0.474, 0.243, 0.18
T'_{d0} , T''_{d0} , T'_{q0}	1.01, 0.053, 0.071
Turbine permanent droop R_P	0.04
Turbine time constant T_w	2.67 s
Servo-motor time constant	0.07 s
Exciter regular gain	400
Exciter time constant	0.01 s

inertia support during the initial stage of the disturbance, hindering the ROCOF and preventing the AC frequency from falling rapidly. From Fig. 8(a) and Fig. 8(b), it is noted that with the power- frequency droop control, the frequency nadir is lifted higher, but the improvement of ROCOF is not obvious at the first few seconds of sudden load increase. Additionally, the extra power provided by power-frequency droop control is proportional to the frequency deviation as shown in Fig. 8(c). So the goal of power-frequency droop control is to simulate the primary control of SG, providing continuous active power support, preventing the continuous drop of AC frequency, improving the frequency nadir, and allowing frequency to achieve a new balance. It can be seen from Fig. 8 and Table 2 that the proposed coordinated control (case 5) combines the advantages of VCC strategy and power-frequency droop control, which can effectively limit ROCOF and improve the frequency nadir. It can be concluded that the proposed coordinated control enables the PMSG-based WT to provide inertial response and primary control services, which is very meaningful and useful for power systems with high proportions of wind power.

VII. CONCLUSION

This paper has proposed a comprehensive coordinated control strategy for PMSG-based WT system to provide frequency services, including the DC-link inertia control, the VCC strategy and power-frequency droop control. The DC-link inertia control utilizes the electrostatic energy stored in the DC capacitor to provide virtual inertia support. However, the available energy is relatively small, so a larger size capacitor might be needed for a required virtual inertia. Fortunately, the VCC strategy can provide a virtual capacitance much larger than the actual DC capacitance by using the WT's rotor kinetic energy, and is aimed to simulate the inertial response of SG, providing virtual inertia support and hindering the ROCOF during the initial stage of the disturbance. The power-frequency droop control can achieve the following goals by simulating the primary control of SG: providing continuous active power support, preventing the continuous drop of AC frequency and improving the frequency nadir. The simulation results indicate that the ROCOF is mitigated and frequency nadir is improved by adopting the proposed coordinated control strategy. The strategy can improve the overall performance of power system with high proportion of wind energy and promote the development of wind energy utilization.

APPENDIX

See Tables 3 and 4.

REFERENCES

[1] D. Ochoa and S. Martinez, "Fast-frequency response provided by DFIG-wind turbines and its impact on the grid," *IEEE Trans. Power Syst.*, vol. 32, no. 5, pp. 4002–4011, Sep. 2017.
[2] Y. Li, Z. Xu, J. Zhang, and K. P. Wong, "Variable gain control scheme of DFIG-based wind farm for over-frequency support," *Renew. Energy*, vol. 120, pp. 379–391, May 2018.
[3] Y. Li, Z. Xu, and K. P. Wong, "Advanced control strategies of PMSG-based wind turbines for system inertia support," *IEEE Trans. Power Syst.*, vol. 32, no. 4, pp. 3027–3037, Jul. 2017.
[4] Y. Li *et al.*, "A dynamic coordinated control strategy of WTG-ES combined system for short-term frequency support," *Renew. Energy*, vol. 119, pp. 1–11, Apr. 2018.
[5] H. Liu and Z. Chen, "Contribution of VSC-HVDC to frequency regulation of power systems with offshore wind generation," *IEEE Trans. Energy Convers.*, vol. 30, no. 3, pp. 918–926, Sep. 2015.
[6] S. Wang, J. Hu, X. Yuan, and L. Sun, "On inertial dynamics of virtual-synchronous-controlled DFIG-based wind turbines," *IEEE Trans. Energy Convers.*, vol. 30, no. 4, pp. 1691–1702, Dec. 2015.
[7] R. M. Kamel, A. Chaouachi, and K. Nagasaka, "Three control strategies to improve the microgrid transient dynamic response during isolated mode: A comparative study," *IEEE Trans. Ind. Electron.*, vol. 60, no. 4, pp. 1314–1322, Apr. 2013.
[8] Y. Fu, Y. Wang, and X. Zhang, "Integrated wind turbine controller with virtual inertia and primary frequency responses for grid dynamic frequency support," *IET Renew. Power Gener.*, vol. 11, no. 8, pp. 1129–1137, Jun. 2017.

[9] X. Lyu, J. Zhao, Y. Jia, Z. Xu, and K. P. Wong, "Coordinated control strategies of PMSG-based wind turbine for smoothing power fluctuations," *IEEE Trans. Power Syst.*, vol. 34, no. 1, pp. 391–401, Jan. 2019.
[10] Z.-S. Zhang, Y.-Z. Sun, J. Lin, and G.-J. Li, "Coordinated frequency regulation by doubly fed induction generator-based wind power plants," *IET Renew. Power Gener.*, vol. 6, no. 1, pp. 38–47, Jan. 2012.
[11] J. M. Mauricio, A. Marano, A. Gomez-Exposito, and J. L. M. Ramos, "Frequency regulation contribution through variable-speed wind energy conversion systems," *IEEE Trans. Power Syst.*, vol. 24, no. 1, pp. 173–180, Feb. 2009.
[12] H. Ye, W. Pei, and Z. Qi, "Analytical modeling of inertial and droop responses from a wind farm for short-term frequency regulation in power systems," *IEEE Trans. Power Syst.*, vol. 31, no. 5, pp. 3414–3423, Sep. 2016.
[13] J. Van de Vyver, J. D. M. De Kooning, B. Meersman, L. Vandevelde, and T. L. Vandoorn, "Droop control as an alternative inertial response strategy for the synthetic inertia on wind turbines," *IEEE Trans. Power Syst.*, vol. 31, no. 2, pp. 1129–1138, Mar. 2016.
[14] M. Kayikci and J. V. Milanovic, "Dynamic contribution of DFIG-based wind plants to system frequency disturbances," *IEEE Trans. Power Syst.*, vol. 24, no. 2, pp. 859–867, May 2009.
[15] K. V. Vidyanandan and N. Senroy, "Primary frequency regulation by deloaded wind turbines using variable droop," *IEEE Trans. Power Syst.*, vol. 28, no. 2, pp. 837–846, May 2013.
[16] X. Zhang, X. Zha, S. Yue, and Y. Chen, "A frequency regulation strategy for wind power based on limited over-speed de-loading curve partitioning," *IEEE Access*, vol. 6, pp. 22938–22951, 2018.
[17] Y. Li, Z. Xu, J. Zhang, H. Yang, and K. P. Wong, "Variable utilization-level scheme for load-sharing control of wind farm," *IEEE Trans. Energy Convers.*, vol. 33, no. 2, pp. 856–868, Jun. 2018.
[18] P. Li, W. Hu, R. Hu, Q. Huang, J. Yao, and Z. Chen, "Strategy for wind power plant contribution to frequency control under variable wind speed," *Renew. Energy*, vol. 130, pp. 1226–1236, Jan. 2019.
[19] J. Licari, J. Ekanayake, and I. Moore, "Inertia response from full-power converter-based permanent magnet wind generators," *J. Mod. Power Syst. Clean Energy*, vol. 1, no. 1, pp. 26–33, Jun. 2013.
[20] X. Liu, Z. Xu, and J. Zhao, "Combined primary frequency control strategy of permanent magnet synchronous generator-based wind turbine," *Electr. Power Compon. Syst.*, vol. 46, nos. 14–15, pp. 1704–1718, 2019. doi: 10.1080/15325008.2018.1509916.
[21] A. M. Howlader, T. Senjyu, and A. Y. Saber, "An integrated power smoothing control for a grid-interactive wind farm considering wake effects," *IEEE Syst. J.*, vol. 9, no. 3, pp. 954–965, Sep. 2015.
[22] A. D. Hansen and G. Michalke, "Multi-pole permanent magnet synchronous generator wind turbines' grid support capability in uninterrupted operation during grid faults," *IET Renew. Power Gener.*, vol. 3, no. 3, pp. 333–348, Sep. 2009.
[23] M. F. M. Arani and Y. A.-R. I. Mohamed, "Assessment and enhancement of a full-scale PMSG-based wind power generator performance under faults," *IEEE Trans. Energy Convers.*, vol. 31, no. 2, pp. 728–739, Jun. 2016.
[24] J. F. M. Padron and A. E. F. Lorenzo, "Calculating steady-state operating conditions for doubly-fed induction generator wind turbines," *IEEE Trans. Power Syst.*, vol. 25, no. 2, pp. 922–928, May 2010.
[25] Y. Li, Z. Zhang, Y. Yang, Y. Li, H. Chen, and Z. Xu, "Coordinated control of wind farm and VSC-HVDC system using capacitor energy and kinetic energy to improve inertia level of power systems," *Int. J. Elect. Power Energy Syst.*, vol. 59, pp. 79–92, Jul. 2014.
[26] A. Junyent-Ferr, Y. Pipelzadeh, and T. C. Green, "Blending HVDC-link energy storage and offshore wind turbine inertia for fast frequency response," *IEEE Trans. Sustain. Energy*, vol. 6, no. 3, pp. 1059–1066, Jul. 2015.
[27] F. Teng, M. Aunedi, D. Pudjianto, and G. Strbac, "Benefits of demand-side response in providing frequency response service in the future GB power system," *Frontiers Energy Res.*, vol. 3, p. 36, Aug. 2015.
[28] J. Zhu, C. D. Booth, G. P. Adam, A. J. Roscoe, and C. G. Bright, "Inertia emulation control strategy for VSC-HVDC transmission systems," *IEEE Trans. Power Syst.*, vol. 28, no. 2, pp. 1277–1287, May 2013.
[29] P. Kundur, *Power System Stability and Control*. New York, NY, USA: McGraw-Hill, 1994.
[30] G. Delille, B. Francois, and G. Malarange, "Dynamic frequency control support by energy storage to reduce the impact of wind and solar generation on isolated power system's inertia," *IEEE Trans. Sustain. Energy*, vol. 3, no. 4, pp. 931–939, Oct. 2012.

XUEYANG ZENG was born in Sichuan, China, in 1992. He received the B.S. degree from Sichuan University, Chengdu, China, in 2016, where he is currently pursuing the Ph.D. degree with the College of Electrical Engineering and Information Technology.

Since 2018, he has been a joint Ph.D. Student funded by the China Scholarship Council with the Department of Energy Technology, Aalborg University, Aalborg, Denmark. His current research interests include renewable energy integration and high voltage direct current.

TIANQI LIU (SM'16) received the B.S. and the M.S. degrees from Sichuan University, Chengdu, China, in 1982 and 1986, respectively, and the Ph.D. degree from Chongqing University, Chongqing, China, in 1996, all in electrical engineering. She is currently a Professor with the College of Electrical Engineering and Information Technology, Sichuan University. Her research interests include power system analysis and stability control, HVDC, optimal operation, dynamic security analysis, dynamic state estimation, and load forecast.

SHUNLIANG WANG (M'18) received the B.S. and Ph.D. degrees in electrical engineering from Southwest Jiaotong University, Chengdu, China, in 2010 and 2016, respectively. From 2017 to 2018, he was a Visiting Scholar with the Department of Energy Technology, Aalborg University, Denmark. He is currently an Associate Research Fellow with the College of Electrical Engineering and Information Technology, Sichuan University. His current research interests include digital control and modulation of multilevel converters, and high voltage direct current.

YUQING DONG was born in Jiangsu, China, in 1995. She received the B.S. degree from Sichuan University, Chengdu, China, in 2017, where she is currently pursuing the Ph.D. degree with the College of Electrical Engineering and Information Technology.

Her current research interests include high voltage direct current and harmonic instability.

ZHE CHEN (M'95–SM'98–F'18) received the B.Eng. and M.Sc. degrees from the Northeast China Institute of Electric Power Engineering, Jilin, China, in 1982 and 1986, respectively, and the Ph.D. degree from the University of Durham, Durham, U.K., in 1997. He is currently a Full Professor with the Department of Energy Technology, Aalborg University, Denmark. He is also the Leader of Wind Power System Research program with the Department of Energy Technology, Aalborg University, and the Danish Principle Investigator for Wind Energy of the Sino-Danish Centre for Education and Research. His research areas include power systems, power electronics, and electric machines. His main current research interests include wind energy and modern power systems. He has led many research projects and has more than 500 publications in his technical field.